# Understanding the Synergistic Catalytic Effect between $La_2O_3$ and CaO for the $CH_4$ Lean De-$NO_x$ Reaction: Kinetic and Mechanistic Studies

**T. Anastasiadou,[†] L. A. Loukatzikou,[‡] C. N. Costa,[†] and A. M. Efstathiou*[,†]**

*Department of Chemistry, Heterogeneous Catalysis Laboratory, University of Cyprus, P.O. Box 20537, CY1678 Nicosia, Cyprus, and Department of Chemistry, University of Ioannina, Ioannina 45110, Greece*

*Received: March 27, 2005; In Final Form: June 2, 2005*

Doping of $La_2O_3$ crystallites with $Ca^{2+}$ ions significantly enhances the intrinsic rate of NO reduction by $CH_4$ in the presence of 5% $O_2$ at 550 °C compared to pure $La_2O_3$ and CaO solids, while the opposite is true after doping of CaO with $La^{3+}$ ions. It was found that the 5 wt % $La_2O_3$−95 wt % CaO system has one of the highest intrinsic site reactivities (TOF = $8.5 \times 10^{-3}$ $s^{-1}$) reported at 550 °C for the NO/$CH_4$/$O_2$ reaction among metal oxide surfaces. The doping process occurred after first dispersing $La_2O_3$ and CaO crystallites in deionized water heated to 60 °C for 90 min, while the dried material was then ground and heated slowly in air to 800 °C and kept at this temperature for 5 h. The doping process had the effect of creating surface oxygen vacant sites (F-type defects) in the oxide lattices the concentration of which is a function of the wt % $La_2O_3$ used in the mixed oxide system as revealed by photoluminescence and $O_2$ chemisorption studies. According to DRIFTS $^{15}$NO transient isotopic experiments (SSITKA), oxygen vacant sites in $Ca^{2+}$-doped $La_2O_3$ promote the formation of a more active chemisorbed $NO_x$ species ($NO_2^-$) that contributes to the enhancement of reaction rate as compared to pure lanthana, calcium oxide, and $La^{3+}$-doped CaO. These results were supported by the kinetic orders of the reaction with respect to NO and $O_2$ obtained as a function of wt % $La_2O_3$ content in the mixed oxide system. Carbon dioxide (a reaction product) competes for the same oxygen vacant sites to form stable adsorbed carbonate-like species, thus lowering the reduction rate of NO. The dependence of the reaction TOF on the wt % $La_2O_3$ loading at 550 °C was found to follow the trend of the dependence of photoluminescence intensity on the wt % $La_2O_3$ content in the $La_2O_3$−CaO oxide system.

## Introduction

The selective catalytic reduction of NO by hydrocarbons (HC−SCR) under strongly oxidizing conditions (lean de-$NO_x$) has attracted great attention since the pioneering work of Held et al.[1] and Iwamoto,[2] who independently found that alkanes and alkenes are able to reduce NO over Cu−ZSM5. Thorough review papers on the research on hydrocarbon lean de-$NO_x$ catalysis have appeared.[3−5] Methane is of particular interest as a reductant hydrocarbon species because of the large availability of natural gas, the use of the latter at gas-fired power plants (main stationary $NO_x$ polluting source), and the potential to be considered as an alternative to $NH_3$ reductant used in industrial practice ($NH_3$−SCR technology), which faces various problems.[6]

The lean de-$NO_x$ catalysts so far reported concern (i) zeolites, (ii) supported noble metals, and (iii) metal oxides.[3] Zeolite-based catalysts, such as Cu/ZSM-5 and Co/ZSM-5, have shown promising activity in the SCR of NO by hydrocarbons.[3,7,8] These catalysts present a volcano-type profile of activity versus temperature and they suffer from serious deactivation by the presence of water and $SO_2$[3]. On the other hand, supported noble metals show high catalytic activity at low temperatures for the HC−SCR. However, they exhibit unacceptable selectivity toward $N_2$, a narrow activity versus temperature profile, and a high cost.[3] Inexpensive metal oxides could be seen as potential materials for an HC−SCR of $NO_x$ at temperatures of practical interest that hopefully will not have the drawbacks of the other two classes of materials mentioned above.

Vannice and co-workers[9−17] have extensively studied a wide series of metal oxides such as rare-earth oxides (REOs) and alkaline-earth oxides for the SCR of NO by methane in both the presence and absence of oxygen. Unlike zeolites, the activity of these oxides increases monotonically with temperature and no bend-over in activity was observed up to 700 °C. They have recently reported that $La_2O_3$ is one of the most active REO catalysts.[9,11,14,15] The $N_2$ formation rates (per gram basis) of the REO catalysts were found to be lower than those of zeolite-type because of the low surface area of the former catalysts. However, the intrinsic activity (TOF, $s^{-1}$) of REO materials is similar or higher than that obtained in zeolite-type catalysts. On the basis of these results, certain inexpensive metal oxides could be seen as potential catalysts for the application of the HC−SCR process in the 500−700 °C range, if ways are found to increase their intrinsic reaction rate in terms of TOF ($s^{-1}$) and per gram-basis. Shi et al.[10] and Huang et al.[17] have shown that dispersing $La_2O_3$ on $Al_2O_3$ significantly enhances the rate of NO reduction by $CH_4$ in the presence of oxygen compared to unsupported $La_2O_3$.

We have recently reported catalytic and kinetic results of the NO/$CH_4$/$O_2$ reaction on pure CaO,[18] $La_2O_3$−CaO mixed oxides,[19] La−Sr−Ce−Fe−O oxidic/perovskitic systems,[20] and Mn-based oxidic systems.[21,22] It was shown that CaO is the most active alkaline-earth oxide,[18] while $La_2O_3$ is one of the most

* Address correspondence ot this author. E-mail: efstath@ucy.ac.cy. Fax: (+357) 22 89 2801.
[†] University of Cyprus.
[‡] University of Ioannina.

10.1021/jp0515582 CCC: $30.25 
Published on Web 06/28/2005

active rare-earth oxides[10] for the $NO/CH_4/O_2$ reaction. A largely positive synergistic catalytic effect between $La_2O_3$ and CaO due to doping of lanthana with $Ca^{2+}$ ions at 800 °C was observed in the 5 wt % $La_2O_3$−95 wt % CaO system for the $NO/CH_4/O_2$ reaction at 550 °C.[19]

The present work concerns kinetic and mechanistic studies of the NO reduction by methane under strongly oxidizing conditions (5−10 mol %) on *x* wt % $La_2O_3$−CaO mixed metal oxides in order to elucidate some intrinsic kinetic reasons for the existence of a synergistic catalytic effect between the two metal oxide phases, which depends on reaction conditions and $La_2O_3$ content.[19] Photoluminescence studies have shown that the presence of F-type defects in the $La_2O_3$−CaO system correlates well with their catalytic performance. Moreover, transient isotopic experiments (SSITKA, use of $^{15}NO$) were conducted with in situ Diffuse Reflectance Infrared Fourier Transform Spectroscopy (DRIFTS) to elucidate the chemical structure of adsorbed *active and inactive* (spectator) $NO_x$ species under $NO/CH_4/O_2$ reaction conditions and relate this information with the synergistic catalytic effect. On the basis of these results, a critical comparison of the effects of catalyst chemical composition on key aspects of the reaction mechanism was made. Detailed work previously reported from this laboratory[19] and which was mainly focused on the chemical interaction of NO, $O_2$, and $CO_2$ with the present catalytic surfaces confirmed the strong relationship between F-type defects and chemisorptive/catalytic properties but also the synergy exhibited by CaO and $La_2O_3$ phases toward the $NO/CH_4/O_2$ catalytic reaction.

## Experimental Section

**Catalyst Preparation.** Weighted amounts of CaO and $La_2O_3$ (Aldrich, 99.999%) corresponding to the desired composition were placed in a glass beaker containing deionized water and heated to 60 °C under continuous stirring. After about 90 min of stirring, the slurry obtained was dried at 120 °C for 24 h. The dried material was well ground and then placed in an oven the temperature of which was raised stepwise to 800 °C. The material was kept at 800 °C for 5 h, cooled in air to room temperature, and stored for further use.

**Catalyst Characterization.** The specific surface areas of the solid catalysts were measured by using the BET method (Micromeritics 2100E Accusorb instrument) with nitrogen as adsorbate gas. X-ray powder diffraction patterns of the *x* wt % $La_2O_3$−CaO solids were obtained after calcination at 800 °C, using a Philips 1830/40 diffractometer with Cu Kα radiation ($\lambda = 1.5415$Å) and Ni filter (0.4 in. incoming slit). The surface morphology of the catalysts was examined through a JEOL JSM 5200 scanning electron microscope at the voltage of 25 kV. Powdered specimens were spread on the SEM slabs sputtered with gold. Results of these characterization studies have been reported.[19]

**Kinetic Studies.** The flow system used for performing kinetic and mechanistic studies for the $CH_4/NO/O_2$ reaction at 1 atm total pressure consisted of a flow measuring and control system (mass flow controllers, MKS Instruments, Model 247C), mixing chambers, a quartz fixed-bed microreactor (2 mL nominal volume), a GC-MS analysis system, and $NO_x$ (chemiluminescence) and $CO_2$ (infrared) analyzers. The flow system, the microreactor, and the GC-MS analysis system used have been described in detail.[19,23] The feed stream compositions used for kinetic studies were as follows. Nitric oxide (NO) varied in the 500−6700 ppm range, $CH_4$ in the 0.67−3.0 mol % range, and $O_2$ in the 2−10 mol % range, while He was used as the balance gas. The amount of catalyst used was varied between 50 and 100 mg so as to keep the NO conversion below 15% and that of $CH_4$ below 20−25% in the 500−750 °C range at a total flow rate of 50 NmL/min. A reaction time of 30 min was allowed at each reaction condition before kinetic measurements were recorded. The fresh catalyst sample was first pretreated in $5\%O_2$/He at 800 °C for 4 h.

Intrinsic $N_2$ production and NO consumption rates were calculated from the product analyses by using the differential reactor approximation, $\text{Rate}_{N_2}$ ($\text{mol}\cdot\text{g}^{-1}\cdot\text{s}^{-1}$) $= F_T y_i/W$ and $\text{Rate}_{NO} = F_T y_{NO}^{f} X_{NO}/W$, where $F_T$ is the total molar flow rate (mol/s), $y_i$ is the molar fraction of component i (e.g., $N_2$) expressed in ppm × $10^{-6}$, $X_{NO}$ is the conversion of NO, $y_{NO}^{f}$ is the molar fraction of NO in the feed, and *W* is the weight of catalyst (g).

Turnover frequencies (TOF, $s^{-1}$) of reaction were calculated based on the irreversible amount (mol/g) of NO chemisorption, a procedure also used in the literature for kinetic studies similar to the present catalytic systems. For the present *x* wt % $La_2O_3$−(100 − *x*) wt % CaO systems, the irreversible amounts of NO used were 19.4, 19.8, 19.7, 23.0, 23.9, and 12.4 μmol NO/g for 0, 5, 20, 50, 80, and 100 wt % $La_2O_3$ content, respectively.[19]

For the present catalytic reaction system the following reaction network is considered:

$$2NO + CH_4 + O_2 \rightarrow N_2 + CO_2 + 2H_2O \quad (1)$$

$$2NO + CH_4 + {}^3/_2O_2 \rightarrow N_2O + CO_2 + 2H_2O \quad (2)$$

$$CH_4 + 2O_2 \rightarrow CO_2 + 2H_2O \quad (3)$$

The only N-containing product species formed in the present catalytic reaction were found to be $N_2$ and $N_2O$ with the latter in only small amounts (selectivity to $N_2$ >95%).

**Photoluminescence Studies.** The $La_2O_3$−CaO mixed metal oxide solids after calcination in air at 800 °C for 5 h were quickly removed from the furnace for photoluminescence measurements. The photoluminescence of the solid was recorded at room temperature in air on a Perkin-Elmer LS-3 fluorescence spectrometer equipped with a 8.3 W xenon lamp, a side window photomultiplier tube (Burle 931A), and reflection grating monochromators with fixed slits (10 nm). The wavelength accuracy was ±2 nm and the scanning rate was 120 nm/min. Excitation spectra were corrected for the Xenon lamp intensity as well as for the excitation monochromator efficiency. The spectral band maxima were identified by point-to-point measurements of the luminescence intensity versus wavelength in the range of interest.

**In Situ Transient DRIFTS.** Diffuse Reflectance Infrared Fourier Transform (DRIFT) spectra were recorded on a Perkin-Elmer GX II FTIR spectrophotometer at a resolution of 1 $cm^{-1}$ and after using a high-temperature/high-pressure temperature controllable DRIFTS cell (Spectra Tech) equipped with ZnSe IR windows. About 30 mg of catalyst in well ground powder form and a total flow rate of 50 NmL/min were used in the DRIFTS cell. Before any measurements were taken, the catalyst sample was pretreated in situ in $20\%O_2$/He at 700 °C for 2 h. The feed was then switched to Ar gas at 700 °C for 15 min and the sample was cooled to the appropriate temperature of the experiment to be followed. For FTIR single-beam background subtraction, the spectrum of the catalyst (in oxidized state) was taken in Ar flow. FTIR spectra were collected at the rate of 1 scan/s in the 400−3000 $cm^{-1}$ range and the averaged spectrum (based on 40 spectra collected) was recorded. All spectra were analyzed by using the instrument's Spectrum for Windows software.

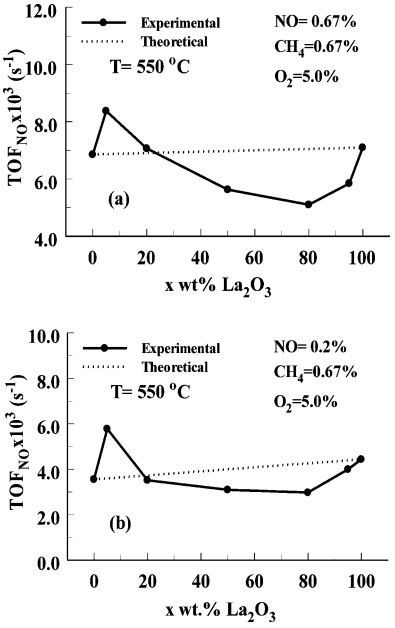


**Figure 1.** Site reactivity (TOF, $s^{-1}$) at 550 °C as a function of $La_2O_3$ content in the *x* wt % $La_2O_3$−CaO mixed metal oxide system. (a) Feed composition: $CH_4$ = 0.67 mol %, NO = 0.67 mol %, $O_2$ = 5 mol %; (b) $CH_4$ = 0.67 mol %, NO = 0.2 mol %, $O_2$ = 5 mol %. GHSV= 65.000 $h^{-1}$.

## Results

**Kinetic Studies.** *Intrinsic Reaction Rates as a Function of* $La_2O_3$ Content. Kinetic experiments have been conducted to determine the relationship between the intrinsic site reactivity (TOF, $s^{-1}$) and the lanthana content (*x* wt %) in the $La_2O_3$−CaO mixed oxide system. This relationship is compared with that predicted by the following eq 4:

$$\mathrm{TOF_m} = (x/100)\cdot\mathrm{TOF_{La_2O_3}} + (1 - (x/100))\cdot\mathrm{TOF_{CaO}} \quad (4)$$

Equation 4 allows the site reactivity of the mixture of the two solid phases ($TOF_m$) to be calculated based on the individual rates of each phase and the content (*x* wt %) of $La_2O_3$ in the mixture. If there is no cooperation (synergy) between the two phases, the experimental rate estimated for the mixture of the two solids must also be predicted by eq 4.

Figure 1 presents the intrinsic TOF of NO consumption as a function of catalyst composition at 550 °C for two reaction feed compositions (different $CH_4$/NO molar ratio). All the mixed oxides with $La_2O_3$ content higher than 20 wt % exhibit lower rates than those predicted by the mixing rule (eq 4), thus, a negative synergistic effect is obtained. However, at a lower $La_2O_3$ content (5 wt %), a different behavior is observed (Figure 1). The experimental site reactivity obtained is significantly higher than that predicted by the mixing rule and, thus, a positive synergistic catalytic effect is observed. It is noted that the 5 wt % $La_2O_3$−CaO solid appears to have the highest TOF value at 550 °C for both feed compositions. This value corresponds to $8.5 \times 10^{-3}$ $s^{-1}$, while the lowest TOF obtained on pure CaO corresponds to $3.6 \times 10^{-3}$ $s^{-1}$.

*Reaction Orders with Respect to NO,* $CH_4$, *and* $O_2$. The reaction orders with respect to NO, $CH_4$, and $O_2$ were evaluated by kinetic experiments at 550 and 750 °C on the 5 and 20 wt % $La_2O_3$−CaO mixed oxide solids. These temperatures were chosen since a bend-over in activity was observed in the 600−700 °C range.[24] Figure 2a presents results of the intrinsic rate of NO consumption as a function of NO concentration at 550 and 750 °C for the 5 wt % $La_2O_3$−CaO catalyst. The

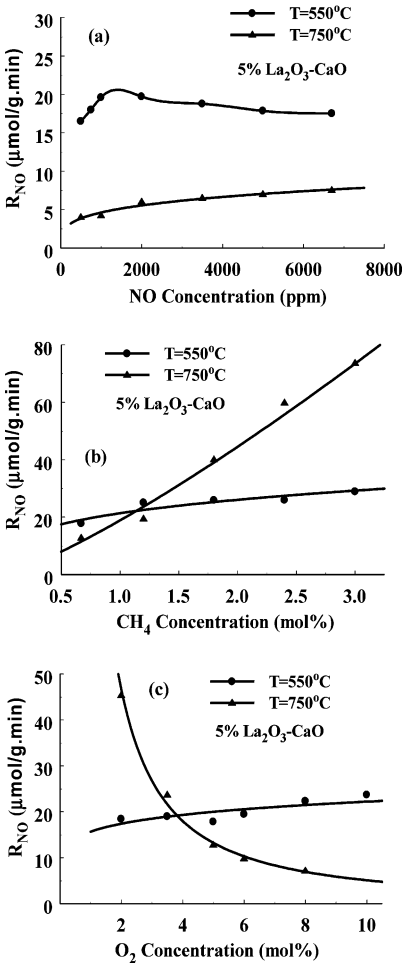


**Figure 2.** Intrinsic rates of NO consumption ($\mu$mol/g·min) as a function of (a) NO concentration, (b) $CH_4$ concentration, and (c) $O_2$ concentration in the feed obtained on the 5 wt % $La_2O_3$−95 wt % CaO solid at 550 and 750 °C.

reaction order with respect to NO was found to be 0.24 at 750 °C. However, at 550 °C a change in the reaction order is obtained with increasing NO concentration. A positive reaction order of 0.25 is obtained in the 500−1000 ppm of NO range, while a slightly negative order is obtained in the 2000−6700 ppm of NO range. A higher reaction order with respect to NO, namely 0.83, was found for the 20 wt % $La_2O_3$−CaO solid at 750 °C. Also, a change in the reaction order with respect to NO was observed at 550 °C in the 500−7000 ppm range. A reaction order of 0.23 was found in the 500−1500 ppm of NO range, while a negative value of −0.1 is obtained in the 2000−6700 ppm range.

Kinetic results for determining the reaction orders with respect to $CH_4$ and $O_2$ for the 5 wt % $La_2O_3$−CaO solid are presented in Figure 2, parts b and c, respectively, at 550 and 750 °C. A large change in the reaction order with respect to $CH_4$ and $O_2$ was observed upon increasing the reaction temperature from 550 to 750 °C. For example, a change in the reaction order with respect to $CH_4$ from 0.29 to 1.24 (Figure 2b) and with respect to $O_2$ from 0.12 to −1.15 (Figure 2c) is observed. All reaction orders with respect to the three reactants for the 5 and 20 wt % $La_2O_3$−CaO catalysts are summarized in Table 1.

*Apparent Activation Energies.* The apparent activation energy ($E_{app}$) of the reaction based on the NO consumption rate for the 5 and 20 wt % $La_2O_3$−CaO catalysts was estimated based on kinetic measurements performed in the 550−680 °C range (0.67% NO/0.67% $CH_4$/5% $O_2$/He) and after using the Arrhenius relationship. Apparent activation energy values of 13.2 (*s* =

**TABLE 1: Reaction Orders[a] with Respect to NO, $CH_4$, and $O_2$ on 5 and 20 wt % $La_2O_3$−CaO Catalysts at 550 and 750 °C**

| catalyst | *x* | | *y* | | *z* | |
|---|---|---|---|---|---|---|
| wt % $La_2O_3$ | 550 °C | 750 °C | 550 °C | 750 °C | 550 °C | 750 °C |
| 5 | 0.25[b] | 0.24 | 0.29 | 1.24 | 0.12 | −1.15 |
| | −0.08[c] | | | | | |
| 20 | 0.23[b] | 0.83 | 0.53 | 1.70 | −0.01 | −1.31 |
| | −0.1[c] | | | | | |

[a] $Rate_{NO} = kP_{NO}^{x} \cdot P_{CH_4}^{y} \cdot P_{O_2}^{z}$. [b] NO concentration was varied in the 500−1500 ppm range. [c] NO concentration was varied in the 2000−6700 ppm range.

0.97) and 17.8 kcal/mol ($s = 0.98$) were obtained for the 5 and 20 wt % $La_2O_3$−CaO solids, respectively.

**Mechanistic Studies.** *Photoluminescence Experiments.* The emission spectra of the *x* wt % $La_2O_3$−(100 − *x*) wt % CaO mixed oxide solids ($x = 0$, 5, 20, 50, 80, 95, and 100) in powder form excited by 200, 220, and 240 nm light are shown in Figure 3, parts a, b, and c, respectively. In general, broad emission bands in the 300−650 nm region were recorded, consisting of at least six overlapping components. The spectral features of all solids appear to be similar, although differences are observed in the overall and the relative band intensities and also in the energy maxima.

Excitation of the *x* wt % $La_2O_3$−CaO solids at 200 (Figure 3a) and 220 nm (Figure 3b) gives rise mainly to indigo emission at $\lambda_{max} = 420$−425 nm and $\lambda_{max} = 417$−422 nm, respectively. Excitation at 240 nm (Figure 3c) results mainly in violet emission ($\lambda_{max} = 385$−388 nm). The four main emission bands recorded after excitation in the 200−240 nm region exhibit maxima in the violet (371−392 nm), indigo (414−425 nm), blue-green (482−491 nm), and green (526−531 nm) regions depending on the excitation wavelength and the solid composition. Two other emission peaks were clearly recorded after excitation at 200 or 220 nm at the blue (440−447 nm) and orange (622−627 nm) regions of the spectra, while a shoulder in the ultraviolet (314−329 nm) region is also present. This shoulder appears as a resolved peak at 307−312 nm in the spectra recorded upon excitation at 240 nm (Figure 3c). It is noted that the known luminescence of $La_2O_3$[25] at 570−650 nm ($\lambda_{max} = 630$ nm) that arises after excitation at 280−320 nm ($\lambda_{max} = 295$ nm) was not recorded by the experimental procedure followed here.

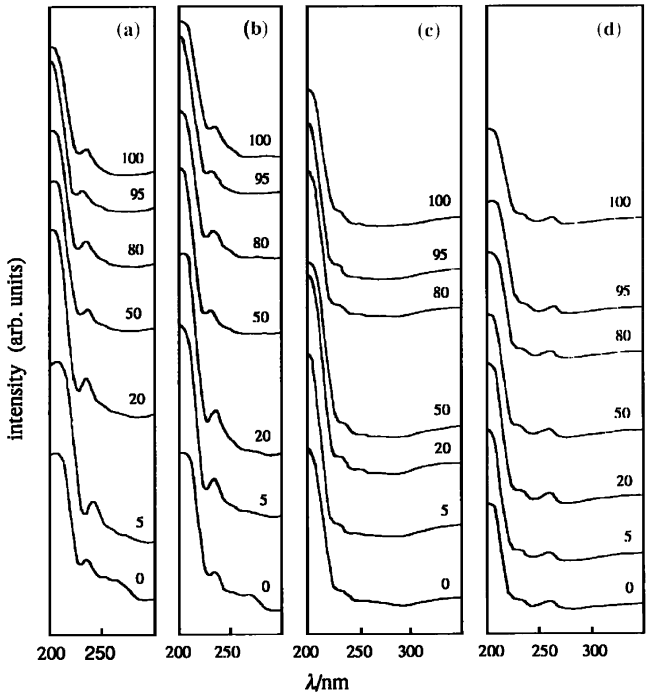


**Figure 4.** Excitation spectra of (a) $\lambda_{em} = 370$ nm, (b) $\lambda_{em} = 420$ nm, (c) $\lambda_{em} = 485$ nm, and (d) $\lambda_{em} = 530$ nm luminescence on *x* wt % $La_2O_3$−CaO mixed oxide solids.

The excitation spectra of the *x* wt % $La_2O_3$−CaO mixed oxides are shown in Figure 4. All excitation spectra recorded for $\lambda_{em} = 370$, 420, 485, and 530 nm (Figure 4a−d) show a broad band with a maximum at 200−206 nm and a second weak band at 230−238 nm that depends on the emission wavelength

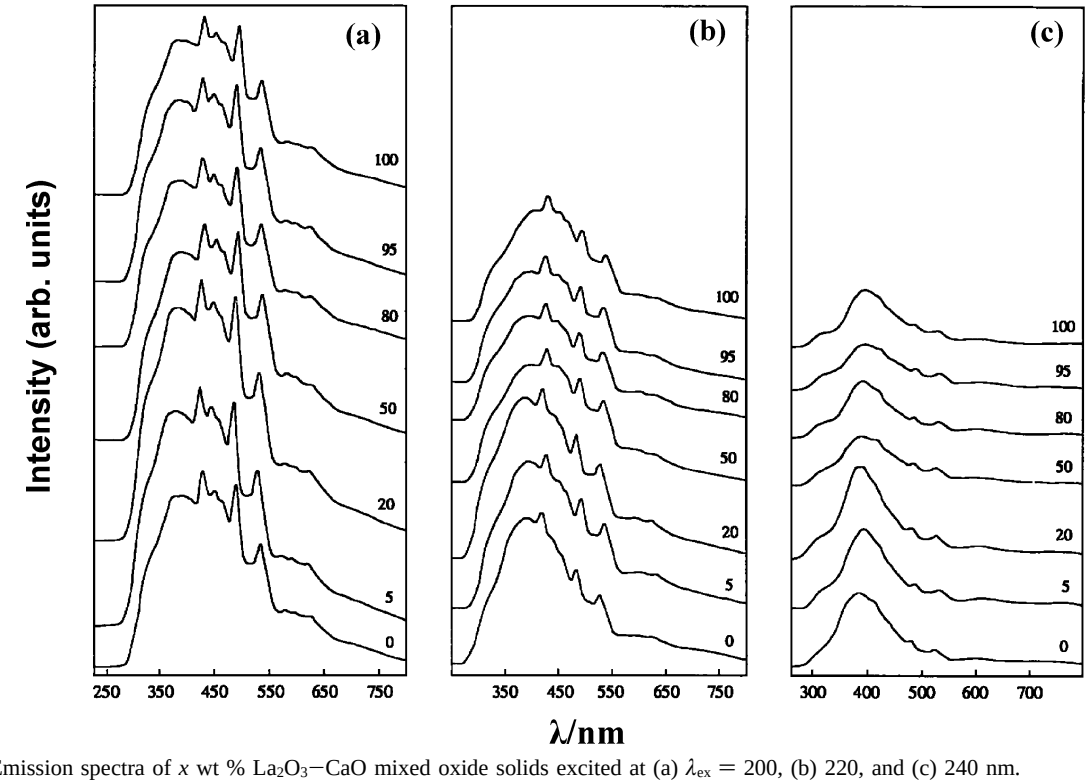


**Figure 3.** Emission spectra of *x* wt % $La_2O_3$−CaO mixed oxide solids excited at (a) $\lambda_{ex} = 200$, (b) 220, and (c) 240 nm.

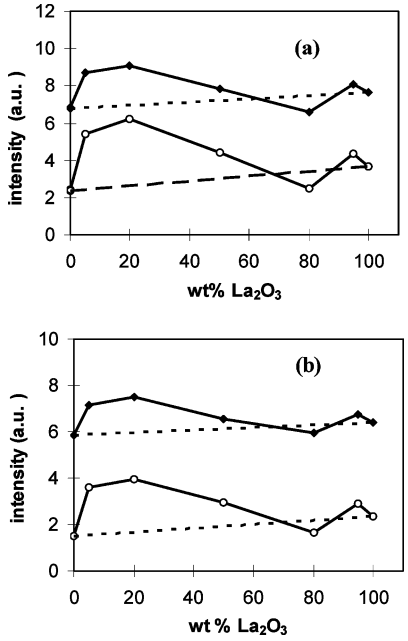


**Figure 5.** Photoluminescence intensity versus wt % $La_2O_3$ content profiles obtained on the *x* wt % $La_2O_3$−CaO solids. The main (indigo or violet (○) and green (◆)) emission intensities were recorded after excitation at 200 (a) and 240 nm (b). The dashed lines correspond to the theoretical mixing rule.

and solid composition. Furthermore, two weaker excitations were recorded at 250−255 and 260−270 nm as shoulders in some emission spectra. In the former case, this leads exclusively to violet ∼ blue-green emission, while this is absent in the excitation spectra recorded for $\lambda_{em} = 530$ nm. The second excitation at 260−270 nm creates a clear band in all excitation spectra recorded at 530 nm (Figure 4d). The intensities of the main (indigo or violet) as well as of the corresponding green emission peaks recorded were found to vary with increasing $La_2O_3$ content as shown in Figure 5, parts a and b, after excitation at 200 and 240 nm, respectively. The variation of emission intensity with lanthana content is found to be nonlinear with local maxima and minima.

*In Situ Transient Isotopic DRIFTS Experiments.* The chemical structure of the adsorbed *active and inactive* (spectator) intermediate $NO_x$ species formed on the surface of *x* wt % $La_2O_3$−CaO mixed oxide solids during $NO/CH_4/O_2$ reaction at 550 °C was studied by in situ DRIFTS. The reaction feed consisted of 0.67% NO, 0.67% $CH_4$, 5% $O_2$, and Ar as a balance gas. The assignment of the IR absorption bands was made based on the literature.[26−37] Table 2 presents the chemical structure and absorption bands (stretching mode) of all important adsorbed $NO_x$ and carbonate species observed during the present DRIFTS studies and others reported in the literature. The chemical structure of the *active adsorbed* $NO_x$ species participating in the reaction path of the $NO/CH_4/O_2$ lean de-$NO_x$ reaction was determined by performing steady-state isotopic transient kinetic analysis (SSITKA) experiments. The experimental procedure was as follows. FTIR spectra were first recorded after 30 min of reaction in $^{14}NO/CH_4/O_2$ at 550 °C. The reaction feed stream was then switched to the equivalent isotopic $^{15}NO/CH_4/O_2$ gas mixture and FTIR spectra were recorded after 30 min of continuous reaction.

Figure 6 shows FTIR spectra recorded on the 5 wt % $La_2O_3$−CaO (Figure 6a) and 80 wt % $La_2O_3$−CaO (Figure 6b) catalysts after 30 min of $^{14}NO/CH_4/O_2$/He reaction (—) and after 30 min the switch $^{14}NO/CH_4/O_2$/He → $^{15}NO/CH_4/O_2$/He was made (- - -) at 550 °C. Note that the former solid presents a largely positive synergistic catalytic effect, while the latter solid presents a largely negative one (Figure 1). The IR bands that are shifted to lower wavenumbers after the isotopic switch ($^{15}N-O$ vs $^{14}N-O$ stretching vibrational mode) correspond to the *active* adsorbed surface intermediate $NO_x$ species formed during the $NO/CH_4/O_2$ reaction that eventually form $N_2$ and $N_2O$ gas

**TABLE 2: Chemical Structures and IR Absorption Bands (stretching mode) of Various Adsorbed $NO_x$ and Carbonate Species on $La_2O_3$−CaO Catalysts[26−37]**

| Species | Structure[a] | Wavenumber ($cm^{-1}$) |
|---|---|---|
| Carbon Dioxide | $CO_2$ (g) | 2140 |
| Dimeric NO, $N_2O_2^{n-}$ (n=1,2) |  | 1700-1750<br>1050-1375 |
| Bridged (chelating) carbonates |  | 1680-1710 |
| Bidentate Carbonates | 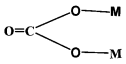 | 1550-1600 |
| Bidentate Nitrates | 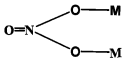 | 1540-1580 |
| Unidentate Carbonates | 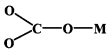 | 1480-1540 |
| Unidentate Nitrates | 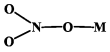 | 1450-1500 |
| Nitritos | 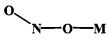 | 1420-1435 |
| Chelating nitrite ($NO_2^-$) | 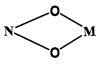 | 1320-1380 (asymmetric) |

[a] M: metal cation on the $La_2O_3$−CaO surface.

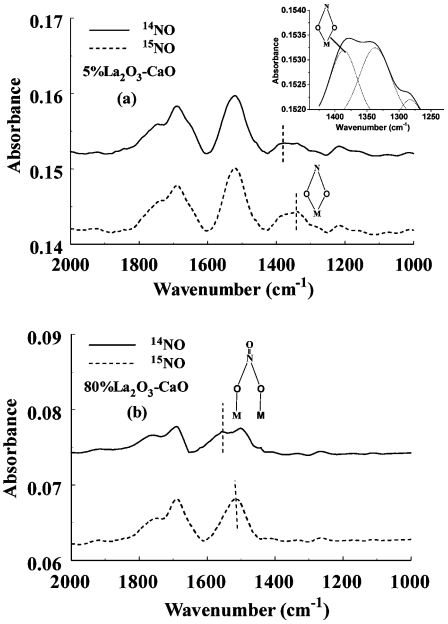


**Figure 6.** In situ DRIFTS spectra recorded over the 5 wt % $La_2O_3$−95 wt % CaO (a) and 80 wt % $La_2O_3$−20 wt % CaO (b) catalysts following $^{14}NO/CH_4/O_2$/Ar reaction at 550 °C for 30 min (—), and after 30 min the isotopic switch $^{14}NO/CH_4/O_2$/Ar → $^{15}NO/CH_4/O_2$/Ar was made at 140 °C (- - -). Feed composition: $CH_4 = 0.67\%$, $NO = 0.2\%$, $O_2 = 5\%$, Ar as balance gas.

products, while those that do not exhibit the isotopic shift correspond to inactive (spectator) $NO_x$ species. However, the likelihood for the presence of *inactive but exchangeable* $NO_x$ species with gaseous $^{15}NO$ cannot be excluded. The shift of IR bands shown by 30−50 $cm^{-1}$ (Figure 6) is consistent with the theory and the work of Beutel et al.[38]

As seen in Figure 6a, four main IR bands were observed in the case of 5 wt % $La_2O_3$−CaO catalyst. The shoulder recorded at 1760 $cm^{-1}$ (Figure 6a) corresponds to $N_2O_2^-$, while the IR band at 1690 $cm^{-1}$ corresponds to *bridged carbonate species*.[16] Deconvolution (Gaussian peak shape) of the IR band observed in the 1600−1420 $cm^{-1}$ range results in two new IR bands at 1550 and 1510 $cm^{-1}$ (not shown). The large band recorded at 1510 $cm^{-1}$ is attributed to *unidentate carbonates*,[16] while that at 1550 $cm^{-1}$ is attributed to *bidentate* nitrates.[35] Deconvolution of the complex IR band observed in the 1430−1250 $cm^{-1}$ range (see inset graph, Figure 6a) results in three new IR bands at 1370, 1330, and 1280 $cm^{-1}$. The IR band at 1370 $cm^{-1}$ corresponds to *chelating nitrite species* ($NO_2^-$), while those at 1330 and 1280 $cm^{-1}$ correspond to *dimeric or polymeric* $N_2O_2^{n-}$ species.[26,32]

As seen in Figure 6a, in the case of 5 wt % $La_2O_3$−CaO only one IR band is shifted to lower wavenumbers after the isotopic switch of the reaction mixture. In particular, the band recorded at 1370 $cm^{-1}$ is shifted to 1330 $cm^{-1}$ and corresponds to *chelating nitrite species* ($NO_2^-$) on $La_2O_3$ and CaO.[26,32,36,37] Therefore, the only *adsorbed active intermediate* $NO_x$ species formed on the 5 wt % $La_2O_3$−CaO catalyst during $NO/CH_4/O_2$ reaction is the *chelating nitrite*. A completely different result was obtained in the case of 80 wt % $La_2O_3$−CaO catalyst (Figure 6b). No infrared bands are observed in the 1300−1400 $cm^{-1}$ range. Therefore, neither $NO_2^-$ nor $N_2O_2^{n-}$ stable species are formed on the 80 wt % $La_2O_3$−CaO catalyst surface during the $NO/CH_4/O_2$ reaction. After deconvolution of the 1600−1400 $cm^{-1}$ band obtained it was found that the only *adsorbed active* $NO_x$ species observed is that of *bidentate nitrate* (1550 $cm^{-1}$). A similar behavior was also observed over the rest of the $La_2O_3$−CaO mixed metal oxides investigated. Summarizing, b*identate* nitrates were found to be the only active intermediate $NO_x$ species formed on the x wt % $La_2O_3$−CaO except on the 5 wt % $La_2O_3$−CaO solid. For the latter, *chelating nitrite species* ($NO_2^-$) were found to be the only *active intermediate* $NO_x$ species (Figure 6a). It will be shown later that formation of *chelating nitrite* ($NO_2^-$) requires the presence of oxygen vacancies (F centers) on the catalyst surface, the formation of which is favored in the 5 wt % $La_2O_3$−CaO solid compared to the rest of the solids investigated.

To gain more fundamental information concerning key aspects of the mechanism of the reaction, and particularly to identify whether the active adsorbed $NO_x$ species formed during the $NO/CH_4/O_2$ reaction *reversibly* interact with gaseous NO (*exchangeable* $NO_x$ species), the following experiment has been designed. After 30 min of $^{14}NO/CH_4/O_2$/Ar reaction at 550 °C, the feed was switched to 0.67%$^{15}NO$/Ar gas mixture and the FTIR spectrum was recorded after 15 min on stream. The purpose of the latter switch was to stop the reaction and simultaneously exchange the reversibly chemisorbed $NO_x$ species with $^{15}NO$ from the gas phase. It was found that none of the observed IR band had shifted to lower wavenumbers (after the appropriate band deconvolution was performed) following the isotopic switch. Therefore, it can be said that among the *active intermediate* $NO_x$ species formed on the 5 and 80 wt % $La_2O_3$−CaO catalysts during the $NO/CH_4/O_2$ reaction none is considered as *reversibly chemisorbed*.

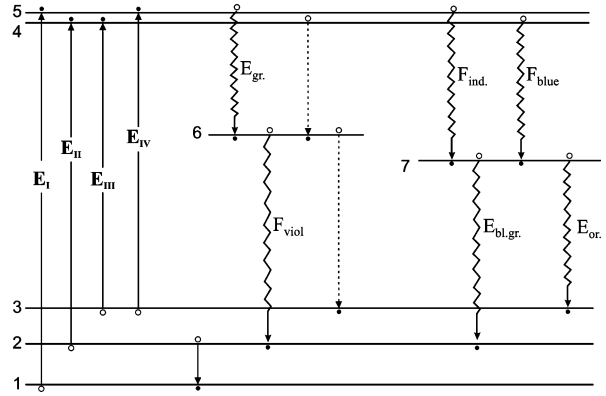


**Figure 7.** General energy diagram describing the photoluminescence (PL) processes occurring on the *x* wt % $La_2O_3$−CaO solids: (●) electron and (○) hole.

**TABLE 3: The Six Main Emission Peaks Recorded over $La_2O_3$−CaO Solids**

| designation[a] | $E_{em}$ (eV) | $\lambda_{em}$ (nm) |
|---|---|---|
| $E_{viol.}$ | 3.34−3.16 | 371−392 |
| $E_{ind.}$ | 2.99−2.92 | 414−425 |
| $E_{blue}$ | 2.82−2.77 | 440−447 |
| $E_{bl.gr.}$ | 2.57−2.52 | 482−491 |
| $E_{gr.}$ | 2.36−2.33 | 526−531 |
| $E_{or.}$ | 2.16−1.98 | 622−627 |

[a] *E* denotes the energy and the subscript the region of each emission peak.

**TABLE 4: The Excitation Peaks Recorded over $La_2O_3$−CaO Solids**

| designation[a] | $E_{ex}$ (nm) | $\lambda_{ex}$ (nm) |
|---|---|---|
| $E_I$ | 6.2−6.02 | 200−206 |
| $E_{II}$ | 5.39−5.21 | 230−238 |
| $E_{III}$ | 5−4.88 | 248−254 |
| $E_{IV}$ | 4.75−4.59 | 261−270 |

[a] *E* denotes the excitation energies.

## Discussion

**The Synergistic Catalytic Effect between CaO and $La_2O_3$ Probed by Photoluminescence Experiments.** A model has been proposed earlier[39] to describe the photoluminescence processes on pure CaO and CaO−ZnO mixed metal oxide systems. In the present work, an improved model is suggested due to the fact that a larger number of resolved spectra were obtained compared to the previous work[39] (at least six peaks are recorded in the present work). The following experimental observations resulted in the general energy diagram depicted in Figure 7. The symbolism used follows the designation given in Tables 3 and 4 that summarize the main emission and excitation peaks, respectively.

$$E_{gr.} + E_{viol.} = E_{ind.} + E_{bl.gr.} \quad (5)$$

$$E_{ind.} - E_{gr.} = E_{viol.} - E_{bl.gr.} \quad (6)$$

$$E_{II} = E_{blue} + E_{bl.gr.} \quad (7)$$

$$E_{III} = E_{ind.} + E_{or.} \quad (8)$$

$$E_{IV} = E_{blue} + E_{or.} \quad (9)$$

Energy level 1 in Figure 7 corresponds to the top of the valence band, while levels 2 and 3 or 4 and 5 correspond to the holes or electron levels generated, respectively. Emission may be the result of several recombination processes between photogener-

ated electrons and holes. Indigo or blue emission is produced during the trapping of one electron by an oxygen anion vacancy, from level 5 or 4, respectively, giving thus rise to the formation of an $F^+$ center. When an additional electron from level 5 is trapped by an oxygen vacancy (e.g., by an $F^+$ center), green emission is produced and an F center is created. Then, the $F^+$ center electron recombines with a hole at level 2 or 3 giving rise to blue-green or orange emission, respectively. When one F-center electron recombines with a hole at level 2, violet emission is produced. Additional processes may also occur according to the dashed vertical lines (Figure 7), giving rise to yellow-green or blue-green emissions, which complete the recombination cycle. It is noted that a yellow-green emission peak is clear in all spectra recorded after excitation at 200 nm (Figure 3). If the above considerations are valid, then energy levels 6 and 7 (Figure 7) correspond to the F- and $F^+$-center levels, respectively.

By applying the photoluminescence (PL) model proposed in Figure 7 for pure CaO and $La_2O_3$, the energy diagrams shown in Figure 8, parts a and b, respectively are obtained. These energy diagrams were made as follows. The experimental energies corresponding to the maxima of the five acute emission bands (indigo, blue, blue-green, green, and orange region) recorded by the 220 nm excitation were first fitted. Next, the energies corresponding to the maxima of the main excitation bands recorded for the emission at 485 nm were fitted. These energy values are given by bold characters in Figure 8a,b. The band gaps of pure oxides used were obtained from literature data.[40,41]

The model agreement to the experimental data is satisfactory in both cases. It is noted that the estimated energy gaps (Figure 8a,b) between electron and hole levels correspond to the maxima of the three weak excitation bands recorded on CaO at 233 (5.32 eV), 253 (4.9 eV), and 261 nm (4.75 eV). A similar behavior is observed on $La_2O_3$ at 231 (5.37 eV), 250 (4.96 eV), and 261 nm (4.75 eV). In addition, the estimated energy gaps between the F and the low-energy hole levels (3.16 eV in both cases) are equal to the violet emission obtained from CaO at 392 nm, and correspond very well to a similar emission obtained from $La_2O_3$ at 390 nm (3.18 eV) also recorded upon excitation of the oxide at 220 nm (Figure 4b).

The secondary excitation energies of $La_2O_3$ recorded at 5.37 or 4.75 eV correspond well to the formation energies of $O^-$ small or large polarons on octahedral positions which were estimated to be 5.37 and 4.73 eV, respectively.[41] Thus, we ascribe the hole levels (Figure 8b) to the $O^-$ holes which are either small or large polaron states on octahedral sites. Also, the estimated energy gap between the more distant hole and electron levels (5.5 eV) (Figure 8b) corresponds well to the energy formation of the $La^{2+}$ defect electron (5.53 eV) in $La_2O_3$.[41] Thus, the higher energy electron level in the case of $La_2O_3$ is probably due to a $La^{2+}$ small polaron state.

It is noted that no corresponding agreement is observed in the case of CaO, e.g., between the luminescence excitation energies and the $O^-$ hole formation energies calculated earlier[42] (4.32 and 5.42 eV for the large and small polaron states, respectively). However, the present results are in good agreement with literature data with respect to the F and $F^+$ level positions. According to the energy diagram of Figure 8a, the F and $F^+$ levels are estimated to be 3.15 and 3.75 eV below the conduction band of CaO, respectively, while the F-center ground level has been found to be 3.11 eV below the conduction band of CaO single crystals.[43] It is noted that the $F^+$ center absorbs at 3.6−3.7 eV.[44−46]

No other crystal phases except of CaO and $La_2O_3$ are present in the solids according to XRD measurements.[19,24] Thus, the photoeffects obtained should be attributed to a synergistic action between the two oxides. In fact, a synergistic action is clear in the PL intensity for the *x* wt % $La_2O_3$−CaO series of solids that is either positive or negative, depending on the $La_2O_3$ content (Figure 5). Thus, in the emission spectra recorded on the 80 wt % $La_2O_3$−CaO (at the main excitation band), a negative synergistic effect is clearly operating in the PL intensity for both excitation energies and for all the emission peaks recorded. However, for the rest of the $La_2O_3$−CaO systems, the synergistic action is clearly positive and especially for the 5 and 20 wt % $La_2O_3$−CaO solids (Figure 5).

The luminescence spectra of *x* wt % $La_2O_3$−CaO solids in air recorded under high-energy UV excitation (Figure 3), although more resolved, are similar to the spectra recorded earlier on CaO and $(CaO)_{1-x}(MO)_x$ (M = Zn, Ti, or Cr) solids.[39,47,48] A similarity is also clear between the spectral features of pure CaO and $La_2O_3$ and those of *x* wt % $La_2O_3$−CaO, despite the differences observed in the total emission and relative band intensities. These results suggest also a similarity in the nature of the photoprocesses involved.

According to the photoluminescence model proposed here, indigo or green emission from the *x* wt % $La_2O_3$−CaO solids represent respectively a measure of the concentrations of $F^+$- or F-type defects that are formed during the illumination. The dominating emission from all the solids is indigo, probably because the recombination processes proceed mainly through the $F^+$ centers. Thus, as a result of the luminescence mechanism considered, the total emission intensity from the solids should be due primarily to the concentration of the oxygen vacancies present in the solids. Namely, the photoluminescence intensity changes observed in the *x* wt % $La_2O_3$−CaO series of solids reflect the alterations in the oxygen vacancy concentration of the solids. This should be especially true for the emissions recorded at the 200 nm excitation (Figure 5a, the main excitation band). The luminescence processes should be more complicated when one excites near the second excitation band (e.g., at 220 or 240 nm). Therefore, according to Figure 5a oxygen anion vacancies are created in $La_2O_3$ by incorporating $Ca^{2+}$ ions and high concentrations of them occur at 80 and 95 wt % CaO content in agreement with the suggestions made[49] that these are the majority compensating defects created in $La_2O_3$ by addition of alkaline-earth metal dopants. A similar but more dramatic effect has been observed by incorporating $Zn^{2+}$ to CaO.[48] On the other hand, oxygen anion vacancies are also created in CaO by incorporating $La^{3+}$. According to the preparation procedure of the present $La_2O_3$−CaO mixed metal oxide system, it is suggested that the presence of a large concentration of CaO crystals in a region of low concentration of $La_2O_3$ crystals (e.g., 5 wt % $La_2O_3$-95 wt % CaO) promotes the formation of a $Ca^{2+}$-doped $La_2O_3$ solid (after calcination at 800 °C for 5 h), while $La^{3+}$-doped CaO is obtained in the case where a large concentration of $La_2O_3$ crystals (e.g., greater than 80 wt %) is present in the homogeneous $La_2O_3$−CaO system.

The above considerations are in harmony with the good correlation that is obtained between the oxygen chemisorption results previously reported on these solids[19] (measure of the concentration of oxygen vacancies) and the main PL intensities. This result is illustrated in Figure 9. A comparison of the above-mentioned results with the intrinsic activity data (Figure 1) leads to the observation that the positive synergistic action coincides between PL intensity ($\lambda_{ex}$ = 200 nm, Figure 5a) and $R_{NO}$ (Figure 1a,b). At the temperature of 550 °C, the increase of catalytic activity of $La_2O_3$ from the addition of 95 wt % CaO is clearly related to the increased concentration of oxygen anion vacancies in the mixed oxide from the presence of $Ca^{2+}$-doped $La_2O_3$ formed. To be more precise, the catalytic activity is related to

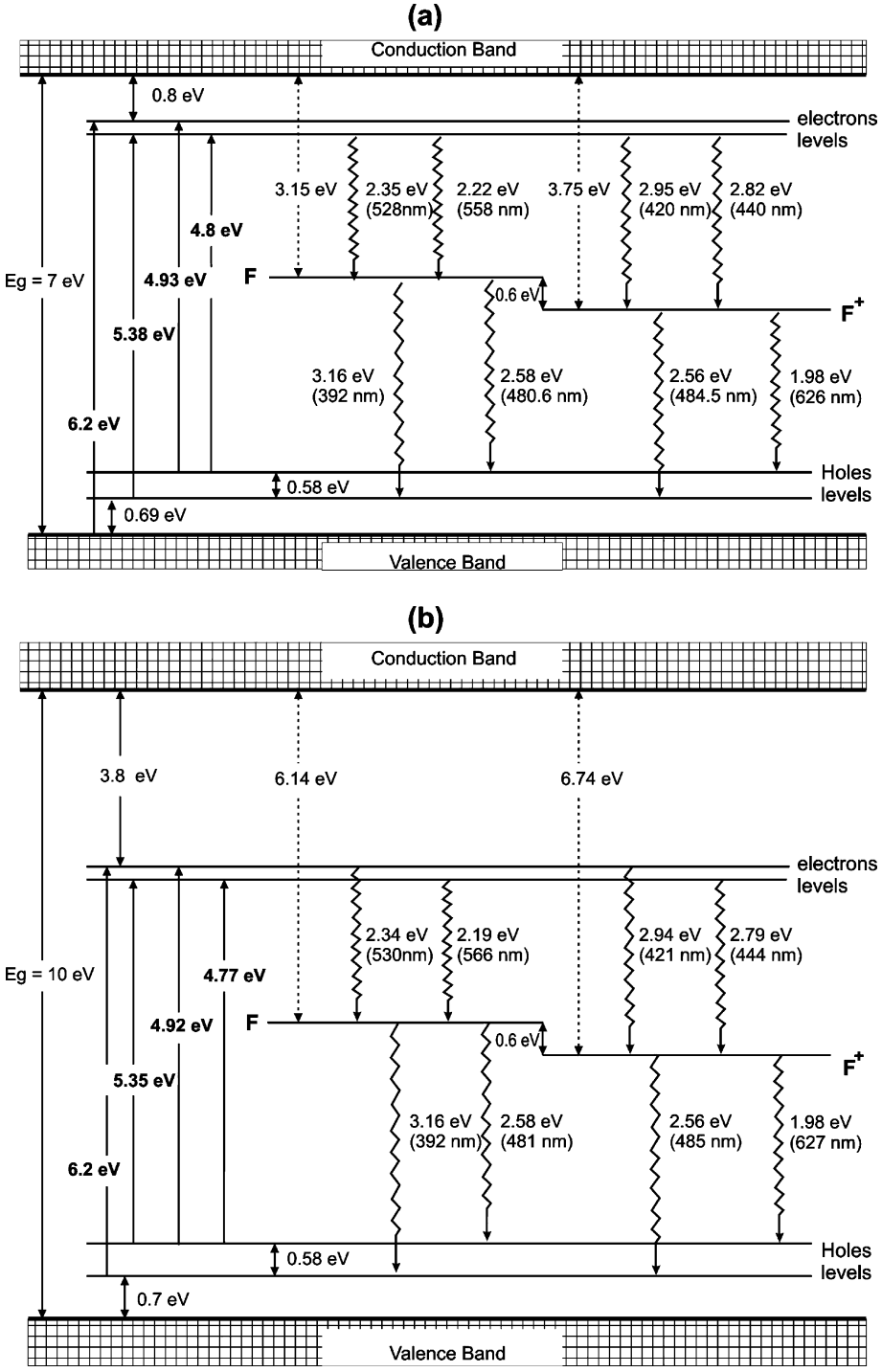


**Figure 8.** Energy diagrams describing the photoluminescence (PL) processes occurring on (a) CaO and (b) $La_2O_3$ solids.

the concentration of $F^+$-type defects, the latter being formed in the solids during illumination via the oxygen anion vacancies. This is shown in Figure 10 where good linear relationships between the photoluminescence intensity ($\lambda_{ex} = 200$ nm) and the intrinsic specific reaction rate of NO consumption at 550 °C for both feed compositions are obtained; a good linear relationship is obtained between the two parameters across the 0−80 wt % $La_2O_3$ loading range (Figure 10).

Although the catalytic activities of the *x* wt % $La_2O_3$−CaO solids were determined under dark conditions, the linear relationships shown in Figure 10 clearly suggest further the possible involvement of $F^+$-type defects. It is pointed out that the intermediate formation of $F^+$ centers is facilitated at room temperature over the $La_2O_3$−CaO oxides during the recombination process, since the dominating emission from the solids is indigo. According to Klingenberg and Vannice,[16] $F^+$-type defects are also formed during the catalytic process over $La_2O_3$ at temperatures higher than 500 °C, via the trapping of one electron by an oxygen anion vacancy. Namely, the electron-transfer processes that facilitate the SCR of NO by $CH_4$ possibly proceed on the solids through oxygen anion vacancies with the intermediate formation of $F^+$ centers. Klingenberg and Vannice[16] also reported that the mechanism of NO decomposition passes through the formation of *chelating nitrite* species on oxygen vacant sites present on $La_2O_3$ surface according to Scheme 1b. Since the 5 wt % $La_2O_3$−CaO solid presents one of the highest amounts of oxygen vacant sites (Figure 5), it is reasonable to suggest that this catalyst will favor the formation of *chelating*

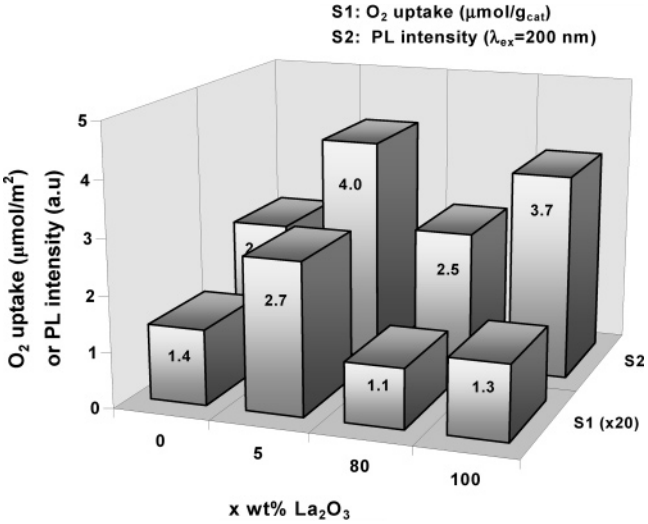


**Figure 9.** Oxygen chemisorption uptake ($\mu$mol/m$^2$) and photoluminescence intensities ($\lambda_{ex}$ = 200 nm) as a function of lanthana content in the *x* wt % $La_2O_3$−CaO solids. A similar pattern is noted.

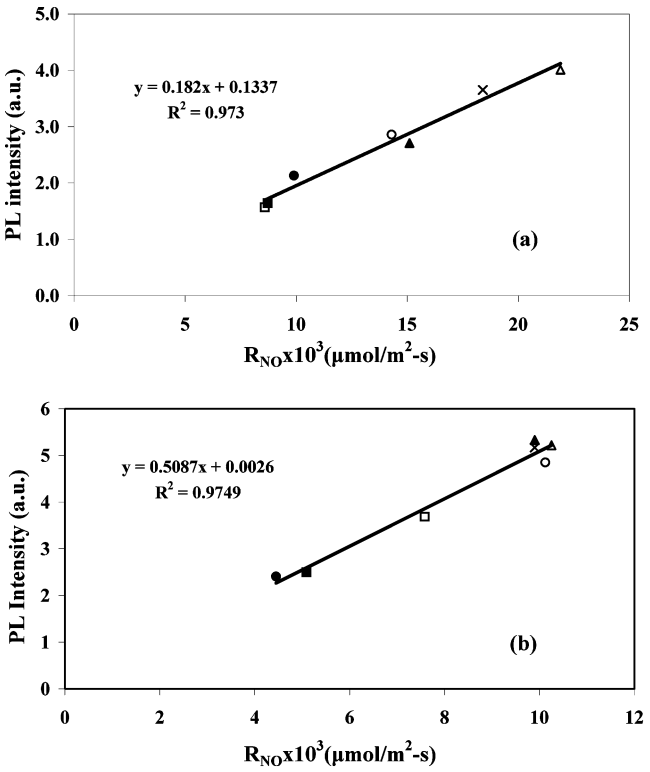


**Figure 10.** Correlation between the intrinsic specific reaction rate of NO consumption ($\mu$mol·m$^{-2}$·s$^{-1}$) at 550 °C and the main photoluminescence intensity on the *x* wt % $La_2O_3$−CaO solids ($\lambda_{ex}$ = 200 nm). Reaction conditions: (a) NO = 0.67 mol %, $CH_4$ = 0.67 mol %, $O_2$ = 5 mol %; (b) NO = 0.2 mol %, $CH_4$ = 0.67 mol %, $O_2$ = 5 mol %.

*nitrites*. The latter result is in good agreement with the results of this work. According to the SSITKA studies performed, *chelating nitrites* ($NO_2^-$) are found to be the only active intermediate $NO_x$ species formed on the 5 wt % $La_2O_3$−CaO catalyst surface, while bridged nitrates (Scheme 1a) are considered as inactive intermediates for the present catalytic reaction.

**The Synergistic Catalytic Effect between CaO and $La_2O_3$ Solids Probed by Kinetic Experiments.** The synergistic action of CaO and $La_2O_3$ phases observed in the present catalytic reaction is clearly demonstrated through the intrinsic kinetic rates of reaction given in Figure 1. The photoluminescence experiments presented and discussed previously provided unambiguous evidence that the oxygen vacancies in the present mixed oxide solid system, largely created by doping of lanthana with $Ca^{2+}$ ions, play a significant role in the observed positive catalytic synergistic effect. These oxygen vacant sites seem to play an important role in the mechanism of the reduction of NO by $CH_4$ under strongly oxidizing conditions (e.g., 5 vol % $O_2$).

**SCHEME 1: Formation of Nitrate and Chelating Nitrite Species on Fully Oxidized (a) and Partially Reduced (presence of oxygen vacant sites) $La_2O_3$ and CaO Solid Surfaces**

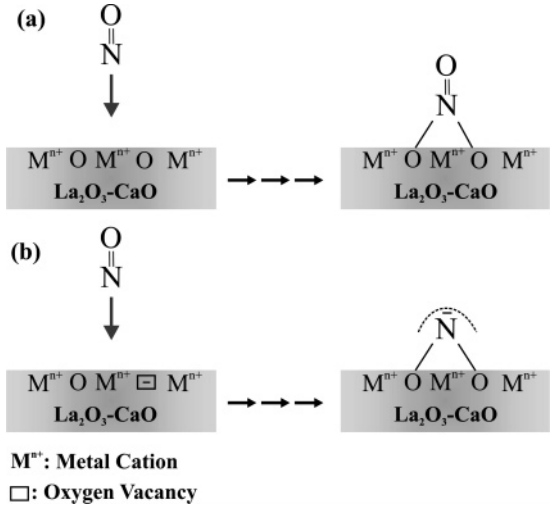


It is known that NO chemisorbs onto oxygen vacant sites forming a different adsorbed state than that formed after chemisorption onto an oxygen anion species (e.g., a surface lattice $O^{2-}$ species) or a metal cation.[16] It is also known that molecular oxygen can adsorb onto oxygen vacancies to form various kinds of negatively charged oxygen species,[50] the latter being responsible for the high activity of metal oxides toward OCM reaction (enhanced rate of $CH_3^\bullet$ radical formation). It has been proposed that reduction of NO by $CH_4$ in the presence of oxygen on $La_2O_3$ surfaces can either pass through an intermediate formed by the interaction of $CH_3^\bullet$ with NO or the formation of $NO_2^-$ intermediate and reduction of the latter to $N_2$.[13] The above-mentioned point out the involvement of oxygen vacancies in more than one elementary steps in the present catalytic reaction mechanism.

It is suggested that the positive synergistic catalytic effect observed on the 5 wt % $La_2O_3$−CaO solid (Figure 1) is mainly due to the involvement of oxygen vacant sites present in the $Ca^{2+}$-doped $La_2O_3$ crystallites toward formation of a more reactive adsorbed intermediate $NO_2^-$ species that is eventually reduced to $N_2$ gas. These chelating nitrite species are only formed over the 5 wt % $La_2O_3$−CaO solid among the rest of the catalysts examined (Figure 6). Moreover, the $NO_2^-$ species is reported to be significantly more active compared to bidentate or unidentate nitrates.[51] The fact that the interaction of $O_2$(g) with surface oxygen vacant sites is very likely to lead to the formation of $O_2^-$ and $O^-$ species on the present catalysts must also be considered.[52,53] In particular, the $O^-$ species can activate $CH_4$ to produce $CH_3^\bullet$ radicals which could interact with adsorbed $NO_x$ to form active intermediate species.[13,54]

The rate of NO reduction by $CH_4$ at low oxygen concentrations ($O_2$ <2 mol %) at 750 °C is found to be more than twice the corresponding rate at 550 °C on the 5 wt % $La_2O_3$−CaO solid (Figure 2c), while at higher $O_2$ concentrations an opposite behavior is observed. This result can be explained based on the following. By decreasing the $O_2$ gas-phase concentration an

**TABLE 5: Comparison of Rates and Reaction Orders of NO Reduction by $CH_4$ in the Presence of $O_2$ on Different Catalysts**

| | reaction conditions | | | | | $R_{N_2}$ ($\mu$mol/s·$g_{cat}$) | reaction orders | | | |
|---|---|---|---|---|---|---|---|---|---|---|
| catalyst | NO (%) | $CH_4$ (%) | $O_2$ (%) | GHSV ($h^{-1}$) | $T$ (°C) | $\times 10^2$ | NO | $CH_4$ | $O_2$ | ref |
| 4% Li/MgO | 2.02 | 0.5 | 1.0 | 3000 | 550 | 0.661 | | | | 12 |
| | | | | | 650 | | | | −0.43 | |
| $La_2O_3$ | 2.02 | 0.5 | 1.0 | 8700 | 500 | 2.9 | | | 0.5[a] | 13 |
| | | | | | 650 | | 0.53 | 0.62 | −0.2[b] | 14 |
| $La_2O_3$ | 0.082 | 0.082 | 0.5 | 8700 | 500 | 0.84 | | | | |
| $Sr/La_2O_3$ | 2.02 | 0.5 | 1.0 | 3300 | 500 | 2.2 | | | | 9 |
| | | | | | 650 | | 0.55 | 0.87 | 0.26 | 14 |
| $Y_2O_3$ | 0.4 | 0.4 | 4.0 | 60000 | 550 | 16.6 | | | | 55 |
| | | | | | 500 | | 0.5 | 0.68 | −0.44 | |
| $Sc_2O_3$ | 0.4 | 0.4 | 4.0 | 60000 | 550 | 17.0 | | | | 55 |
| | | | | | 500 | | 0.44 | 0.92 | −0.61 | |
| 40% $La_2O_3-Al_2O_3$ | 1.8 | 0.45 | 1.0 | 100000 | 550 | 30.0 | | | | 10 |
| 20% $La_2O_3-CaO$ | 0.2 | 0.67 | 5.0 | 33000 | 550 | 4.4 | 0.23 | 0.53 | −0.01 | this work |
| | | | | | 750 | | 0.83 | 1.70 | −1.31 | |
| 5% $La_2O_3-CaO$ | 0.2 | 0.67 | 5.0 | 33000 | 550 | 5.9 | 0.25 | 0.29 | 0.12 | this work |
| | | | | | 750 | | 0.24 | 1.24 | −1.15 | |
| CaO | 0.2 | 0.67 | 5.0 | 33000 | 550 | 3.5 | | | | this work |
| CaO | 0.2 | 2.5 | 2.5 | 20000 | 550 | 2.40 | | | | 18 |
| | | | | | 650 | | 1.0 | 0.5 | 0.25 | |
| Co/ZSM-5 | 0.164 | 0.1025 | 2.5 | 30000 | 500 | 4.58 | | | | 13 |

[a] $P_{O_2} = 0.38-22.8$ Torr, $P_{CH_4} = 25.8$ Torr, $P_{NO} = 15.2$ Torr. [b] $P_{O_2} = 3.8-22.8$ Torr, $P_{CH_4} = 2.67$ Torr, $P_{NO} = 10.65$ Torr.

increase in the surface coverage of oxygen vacant sites is expected, and thus an increase in the coverage of $NO_2^-$ species, the latter being the only active precursor intermediate species of the reaction at hand (Figure 6). The dependence of the rate of NO reduction by $CH_4$ on the $O_2$ concentration (Figure 2c) in the case of 5 wt % $La_2O_3-CaO$ catalyst is found to be in harmony with that reported earlier on pure CaO at 650 and 770°C.[18] The stability with time on stream (24 h) of the rate of NO reduction in the 550−650 °C range for up to 10 mol % $O_2$ concentration on CaO[18] and 5 wt % $La_2O_3-CaO$[24] solids is a remarkable result and of practical interest that has not been reported yet for other metal oxides for the present $NO/CH_4/O_2$ catalytic reaction.

Table 1 clearly indicates that there are significant differences in the orders of reaction between 5 and 20 wt % $La_2O_3-CaO$ catalysts at 750 °C, while at 550 °C these differences become smaller. These results clearly suggest that the active surface intermediate species and/or the nature of rate-controlling step(s) must be different for the two catalytic surfaces. The latter results are in good agreement with the ones obtained by the present SSITKA experiments. According to these experimental studies, completely different kinds of active intermediate $NO_x$ species are formed over the 5 and 20 wt % $La_2O_3-CaO$ catalytic surfaces during the $NO/CH_4/O_2$ reaction. The reactivity toward reduction of the *chelating nitrite species* ($NO_2^-$) on the 5 wt % $La_2O_3-CaO$ solid is expected to be different than that of *bidentate nitrate* formed on the 20 wt % $La_2O_3-CaO$ solid. Large differences in the thermal stability, reactivity toward $CH_4$ and $O_2$, and the nature of decomposition products of these two $NO_x$ species have been reported.[19,26]

An interesting kinetic result obtained in this work is the fact that a reaction order with respect to $CH_4$ higher than unity and a change in reaction order with respect to NO concentration are observed (Table 1). These results seem to suggest the complexity of the kinetics of the present catalytic system. A change in the order of reaction with respect to NO may be due to the fact that the nature of the active intermediate species that is found in the rate-controlling step is influenced by the NO gas-phase concentration. It has been suggested[14] that formation of $CH_3^\bullet$ species by hydrogen abstraction from the $CH_4$ molecule on $Sr/La_2O_3$ and $La_2O_3$ surfaces could occur either via surface negatively charged oxygen or adsorbed $NO_2^-$ species. The coverage of the latter species must depend on the NO gas-phase concentration and temperature (Scheme 1b). For the present case, it was found that adsorbed $NO_2^-$ is indeed formed and this is an active intermediate in the $NO/CH_4/O_2$ reaction path. The formation of the latter species is expected to lead to a decrease in the concentration of surface oxygen species since the formation of *chelating nitrites* ($NO_2^-$) requires oxygen vacancies. It is noted that a similar behavior has been reported for the reaction order with respect to $O_2$ on $La_2O_3$.[13]

The values of reaction order with respect to $CH_4$ obtained at 550 °C for the 5 and 20 wt % $La_2O_3-CaO$ solids are found to be within the 0.3−0.5 range, lower than those observed over other alkaline-earth and rare-earth catalytic surfaces (Table 5). Unfortunately, there are no kinetic studies reported in the literature for the present reaction at 750 °C. This makes impossible the comparison of the values (larger than unity) of reaction order with respect to $CH_4$ obtained in the present work. These values could be related to the fact that the surface coverage of $CNO_xH_y$ adsorbed species formed upon interaction of weakly adsorbed methane with the active $NO_x$ precursor species identified in the present work depends in a positive way on the partial pressure of methane.[54]

The apparent activation energies of reaction at hand estimated for the 5 and 20 wt % $La_2O_3-CaO$ solids are consistent with the values reported for pure CaO (14.6 kcal/mol)[18] and $La_2O_3$ (26 kcal/mol)[14] solids.

The large negative synergistic catalytic effect exhibited by the 80 wt % $La_2O_3-CaO$ solid (Figure 1) is related at least to the different catalytic chemistry of the present reaction exhibited by $La^{3+}$-doped CaO compared to pure $La_2O_3$. Even though the nature of the active $NO_x$ intermediate species for the two catalysts is found to be the same, its surface coverage at steady-state reaction conditions could be different. Furthermore, the importance of the $CO_2$ (product of the reaction) as a poison of active sites for $NO_x$ adsorption in the two catalysts must be considered. Previous studies from our laboratory[19] have clearly demonstrated that $CO_2$ is bound more strongly on 80 wt % $La_2O_3-CaO$ than on pure $La_2O_3$ solid and it significantly prohibits NO chemisorption on the former compared to the latter solid.

**Comparison of Reaction Rates.** Table 5 compares the rates of $N_2$ formation per gram-basis for the $NO/CH_4/O_2$ reaction in the 500−750 °C range over the best alkaline-earth and rare earth-based metal oxides reported. For a more direct comparison

of these results, the feed composition and reaction orders (whenever possible) are also given in Table 5. Results for the Co/ZSM5 zeolitic system are also given. A comparison of the catalytic activity exhibited by $Y_2O_3$[55] and the present 5 wt % $La_2O_3-CaO$ solid reveals the following. After correcting for the differences in the feed compositions used in the two studies, the reaction rate on the 5 wt % $La_2O_3-CaO$ solid at 550 °C and for the feed conditions used (Table 5) is found to be 2.5 times lower than that on $Y_2O_3$. However, it is very important to note that the BET area of $Y_2O_3$ (80 $m^2/g$) is about seven times higher than that of the present 5 wt % $La_2O_3-CaO$ solid (11.0 $m^2/g$).[19] These results demonstrate that the site reactivity of the present catalyst must be considered significantly larger than that of $Y_2O_3$. The activity of 40 wt % $La_2O_3-Al_2O_3$[10] must also be compared with that of the present 5 wt % $La_2O_3-CaO$ solid. At 550 °C, and for the feed conditions used (Table 5), it is found that the activity per gram-basis of the 40 wt % $La_2O_3-Al_2O_3$ solid is about 7 times higher than that of 5 wt % $La_2O_3-CaO$. However, in terms of site reactivity, a TOF of $4.5 \times 10^{-3}$ $s^{-1}$ is calculated for the 5 wt % $La_2O_3-CaO$ compared to $5 \times 10^{-3}$ $s^{-1}$ for the 40 wt % $La_2O_3-Al_2O_3$ solid for the same feed conditions. Therefore, the present catalyst is found to compete favorably for its site reactivity at 550 °C with the best alkaline and rare-earth-based metal oxides reported so far.

**Conclusions.** The present kinetic and mechanistic (photoluminescence and SSITKA) studies have clearly demonstrated the following:

Doping of $La_2O_3$ with $Ca^{2+}$ ions creates active oxygen vacant sites (F-type defects) that are found in the reaction path for the selective reduction of NO by $CH_4$ under strongly oxidizing conditions. The oxygen vacant sites formed facilitate the formation of an active chelating nitrite species ($NO_2^-$) during the $NO/CH_4/O_2$ reaction.

The chemical structure of active adsorbed precursor $NO_x$ intermediate species found in the reaction path from NO to $N_2$ gas ($CH_4/NO/O_2$ reaction) strongly depends on $La_2O_3$ content in the *x* wt % $La_2O_3-CaO$ catalytic system.

$Ca^{2+}$-doped $La_2O_3$ of high specific surface area would be a challenging topic of research for the present lean de-$NO_x$ catalytic reaction in the 500−700 °C range given the low cost of this material.

When the produced $CO_2$ concentration under reaction conditions is high enough, due to the competitive adsorption of NO and $CO_2$ for the same oxygen vacant sites, the rate of poisoning of the catalyst surface by $CO_2$ significantly hinders NO chemisorption.

**Acknowledgment.** Financial support by the Research Committee of the University of Cyprus is gratefully acknowledged.

## References and Notes

(1) Held, W.; Konig, A.; Richter, T.; Puppe, L. *SAE Prepr.* **1990**, No. 900496.

(2) Iwamoto, M. *Proceedings: Meeting on Catalysis Technologies - Removal of NO*, Tokyo, 1990; p 17.

(3) Fritz, A.; Pitchon, V. *Appl. Catal. B* **1997**, *13*, 1.

(4) Burch, R.; Breen, J. P.; Meunier, F. C. *Appl. Catal. B* **2002**, *39*, 283.

(5) Garin, F. *Catal. Today* **2004**, *89*, 255.

(6) Nakajima, F.; Hamada, I. *Catal. Today* **1996**, *29*, 109. Gutberlet, H.; Schallert, B. *Catal. Today* **1993**, *16*, 207.

(7) Li, Y.; Armor, J. N. *J. Catal.* **1994**, *145*, 1.

(8) Amiridis, M. D.; Roberts, K. L.; Perreira, C. J. *Appl. Catal. B* **1997**, *14*, 203.

(9) Zhang, X.; Walters A. B.; Vannice, M. A. *J. Catal.* **1995**, *155*, 290.

(10) Shi, C.; Walters, A. B.; Vannice, M. A. *Appl. Catal. B* **1997**, *14*, 175.

(11) Huang, S. J.; Walters, A. B.; Vannice, M. A. *Appl. Catal. B* **1998**, *17*, 183.

(12) Zhang, X.; Walters, A. B.; Vannice, M. A. *J. Catal.* **1994**, *146*, 568.

(13) Zhang, X.; Walters, A. B.; Vannice, M. A. *Appl. Catal. B* **1994**, *4*, 237.

(14) Vannice, M. A.; Walters, A. B.; Zhang, X. *J. Catal.* **1996**, *159*, 119.

(15) Zhang, X.; Walters A. B.; Vannice, M. A. *Appl. Catal. B* **1996**, *7*, 321.

(16) Klingenberg, B.; Vannice, M. A. *Appl. Catal. B* **1999**, *21*, 19.

(17) Huang, S.-J.; Walters, A. B.; Vannice, M. A. *Appl. Catal. B* **2000**, *26*, 101.

(18) Fliatoura, K. D.; Verykios, X. E.; Costa, C. N.; Efstathiou, A. M. *J. Catal.* **1999**, *183*, 323.

(19) Costa, C. N.; Anastasiadou, T.; Efstathiou, A. M. *J. Catal.* **2000**, *194*, 250.

(20) Belessi, V. C.; Costa, C. N.; Bakas, T. V.; Anastasiadou, T.; Pomonis, P. J.; Efstathiou, A. M. *Catal. Today* **2000**, *59*, 347.

(21) Stathopoulos, V. N.; Belessi, V. C.; Costa, C. N.; Neophytides, S. G.; Falaras, P.; Efstathiou, A. M.; Pomonis, P. J. *Stud. Surf. Sci. Catal.* **2000**, *130*, 1529.

(22) Stathopoulos, V. N.; Costa, C. N.; Belessi, V. C.; Neophytides, S. G.; Pomonis, P. J.; Efstathiou, A. M. *Top. Catal.* **2001**, *16/17*, 231.

(23) Costa, C. N.; Efstathiou, A. M. *J. Phys. Chem. B* **2004**, *108*, 2620.

(24) Anastasiadou, T. Ph.D. Thesis, University of Cyprus, in preparation.

(25) Dmitrienco, A. O.; Akmaeva, I. A.; Rudneva, N. V.; Bolãshakov, A. F. *Inorg. Mater.* **1991**, *27* (5), 823.

(26) Chi, Y.; Chuang, S. C. *J. Phys. Chem. B* **2000**, *104*, 4673.

(27) Rogemond, E.; Essayem, N.; Frety, R. V.; Perrichon, V.; Primet, M.; Chevrier, M.; Gauthier, C.; Mathis, F. *J. Catal.* **1999**, *186*, 414.

(28) Hoost, T. E.; Otto, K.; Laframboise, K. A. *J. Catal.* **1995**, *155*, 303.

(29) Freysz, J.-L.; Saussey, J.; Lavalley, J.-C.; Bourges, P. *J. Catal.* **2001**, *197*, 131.

(30) Garin, F. *Appl. Catal. A* **2001**, *222*, 183.

(31) Morrow, B. A.; Chevrier, J. P.; Moran, L. E. *J. Catal.* **1985**, *91*, 208.

(32) Levoguer, C. L.; Nix, R. M. *Surf. Sci.* **1996**, *365*, 672.

(33) Ryczkowski, J. *Catal. Today* **2001**, *68*, 263.

(34) Binet, C.; Daturi, M.; Lavalley, J.-C. *Catal. Today* **1999**, *50*, 207.

(35) Huang, S.-J.; Walters, A. B.; Vannice, M. A. *Catal. Lett.* **2000**, *64*, 77.

(36) Snis, A.; Panas, I. *Surf. Sci.* **1998**, *412/413*, 477.

(37) Yanagisawa, Y. *Appl. Surf. Sci.* **1996**, *100/101*, 256.

(38) Beutel, T.; Adelman, B. J.; Sachtler, W. M. H. *Appl. Catal. B* **1996**, *9*, L1.

(39) Loukatzikou, L. A.; Sdoukos, A. T.; Pomonis, P. J. *J. Mater. Chem.* **1996**, *6* (5), 887.

(40) Henrich, V. E. *Rep. Prog. Phys.* **1985**, *48*, 1481.

(41) Ilett, D. J.; Islam, M. S. *J. Chem. Soc., Faraday Trans.* **1993**, *89* (20), 3833.

(42) Foot, J. D.; Colbourn, E. A.; Catlow, C. A. R. *J. Phys. Chem. Solids* **1988**, *49* (10), 1225.

(43) Henderson, B.; Stokowski, S. E.; Ensign, T. C. *Phys. Rev.* **1969**, *183* (3), 826.

(44) Hughes, A. E.; Henderson, B. In *Point Defects in Crystals*; Grawford, J. H., Slifkin, L. M., Eds.; Plenum Press: New York, 1972; Vol. 1.

(45) Welch, L. S.; Hughes, A. E.; Summers, G. P. *J. Phys. C: Solid State Phys.* **1980**, *13*, 1791.

(46) Kemp, J. C.; Ziniker, W. M.; Hensley, E. B. *Phys. Lett.* **1967**, *25A* (1), 43.

(47) Loukatzikou, L. A.; Sdoukos, A. T.; Pomonis, P. J. *J. Mater. Chem.* **1997**, *7* (8), 1587.

(48) Loukatzikou, L. A.; Sdoukos, A. T.; Pomonis, P. J. *Catal. Lett.* **1996**, *41*, 113.

(49) Yang, T.; Feng, L.; Shen, S. *J. Catal.* **1994**, *145*, 384.

(50) Busca, G.; Lorenzelli, V. *J. Catal.* **1981**, *72*, 303.

(51) Haneda, M.; Bion, N.; Daturi, M.; Saussey, J.; Lavalley, J.-C.; Duprez, D.; Hamada, H. *J. Catal.* **2002**, *206*, 114.

(52) Acke, F.; Panas, I.; Stromberg, D. *J. Phys. Chem. B* **1998**, *102*, 5127.

(53) Becker, S.; Baerns, M. *J. Catal.* **1991**, *128*, 512.

(54) Sadavskaya, E. M.; Suknev, A. P.; Pinaeva, L. G.; Goncharov, V. B.; Bal'zhinimaev, B. S.; Chupin, C.; Perez-Ramirez, J.; Mirodatos, C. *J. Catal.* **2004**, *225*, 179.

(55) Fokema, M. D.; Ying, J. Y. *Appl. Catal. B* **1998**, *18*, 71.